INSTITUTE OF PHYSICS PUBLISHING JOURNAL OF PHYSICS D: APPLIED PHYSICS

J. Phys. D: Appl. Phys. **37** (2004) 1998–2008 PII: S0022-3727(04)76050-7

A study of dynamic resistance during small scale resistance spot welding of thin Ni sheets

W Tan, Y Zhou, H W Kerr and S Lawson

Department of Mechanical Engineering, University of Waterloo, 200 University Avenue W., Waterloo, Ontario, Canada N2L 3G1

Received 10 February 2004
Published 30 June 2004
Online at stacks.iop.org/JPhysD/37/1998
doi:10.1088/0022-3727/37/14/017

Abstract

The dynamic resistance has been investigated during small scale resistance spot welding (SSRSW) of Ni sheets. Electrical measurements have been correlated with scanning electron microscope images of joint development. The results show that the dynamic resistance curve can be divided into the following stages based on physical change in the workpieces: asperity heating, surface breakdown, asperity softening, partial surface melting, nugget growth and expulsion. These results are also compared and contrasted with dynamic resistance behaviour in large scale RSW.

1. Introduction

In resistance spot welding (RSW) the heat to form a weld is generated by the resistance to the flow of electric current through the sheets being joined. This resistance involves electrode and sheet bulk resistances as well as electrode-to-sheet and sheet-to-sheet contact resistances [1]. The study of the changes in resistance during welding (dynamic resistance) can help in understanding process mechanisms [2], optimizing process parameters [3] and developing quality control strategies [4]. Therefore, dynamic resistance behaviour during RSW has attracted lots of research interest.

There is an increasing demand during fabrication of electronic and medical devices to join very thin metal sheets (thinner than 0.2–0.5 mm), most being similar and dissimilar combinations of non-ferrous metals [5, 6]. This application of RSW, generally termed small scale RSW (SSRSW), requires much more precise electrical and mechanical control, and uses lower electrode force and current/energy input. However, there remains a lack of understanding of SSRSW despite the increasing demand. Conversely, extensive research and development work has been carried out in the area of 'large scale' RSW (LSRSW) of relatively thick sheet steels (thicker than 0.6–0.8 mm) mainly for applications in the automotive and appliance industries [7, 8]. For example, recently most published dynamic resistance studies have been based on LSRSW of steels using a line-frequency ac power supply (see details in the following section), with which the shape of the dynamic resistance curve is suggested to be suitable for quality control. Some of the control strategies developed have been successfully used in industrial production [9]. Compared with LSRSW, limited research has been published on SSRSW, especially on dynamic resistance. The objective of this work is to study the relationship between nugget development and dynamic resistance curves during SSRSW of Ni using a dc power supply.

2. Technical background

Contact resistance is a useful theoretical idealization of the real physical situation. For example, in experiments (figure 1), the measured sheet-to-sheet resistances always include part of the bulk resistance of the sheets [8]. Therefore, the dynamic resistance, R, between two sheets will follow the equation:

$$R = R_C + R_F + R_B \tag{1}$$

where R_C, R_F and R_B are the constriction resistance, film resistance for metals with film or contaminant on the surface and bulk resistance, respectively.

The bulk resistance R_B could be calculated using the following equation:

$$R_B = \rho \frac{l}{A} \tag{2}$$

where ρ is the resistivity, l is the length of current path (one sheet thickness when the two sheets are identical in thickness) and A is the area of current path.

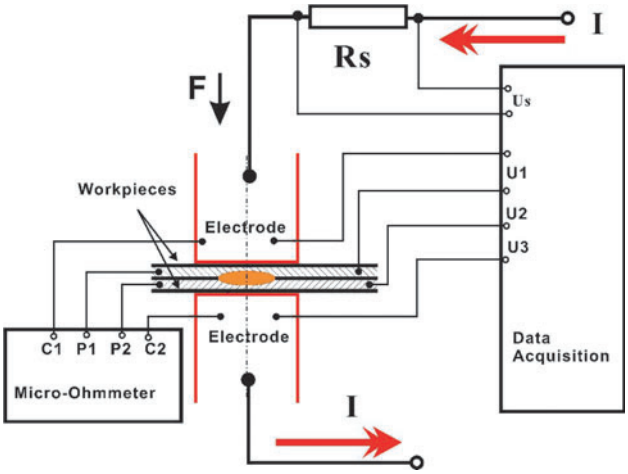

Figure 1. Experimental set-up.
(This figure is in colour only in the electronic version)

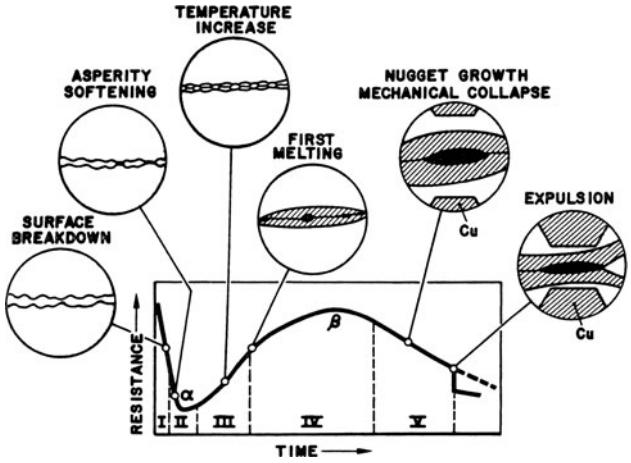

Figure 2. Dynamic resistance during LSRSW of steel [2].

For metals with clean surfaces, the contact resistance is equal to the constriction resistance [10, 11]. The constriction resistance R_C has frequently been found to follow the relationship [10]

$$R_C = 0.89\rho\left(\frac{\xi H}{nF}\right)^{1/2} \tag{3}$$

where ρ is the resistivity of contact spots, H is the hardness, F is the compressive force and ξ is the pressure factor, its value ranges from about $\xi = 0.2$ for surfaces with considerable elastic action to $\xi = 1.0$ for totally plastic contact. A value of $\xi = 0.7$ is often a fair approximation when detailed study is not warranted [11]. n is the contact spot number, polished, well-rounded crossed cylinders tend toward $n = 1$; large, overlapping, flat, electroplated surfaces have values of n more often between 10 and 20 [11].

For metals with film or contaminant on the surfaces, the contact resistance is equal to constriction resistance plus film resistance. In classical theory, when there is a dielectric film on the surface of metal, the electrons will not be able to go through the film. However, according to quantum physics, electrons may be able to pass the film by tunnelling when the film thickness is comparable with the electron mean free paths of metals at room temperature, which are in the range of 50–5000 Å [11]. The film resistance R_F can be written as [10, 11]

$$R_F = \frac{\rho_t \xi H}{F} \tag{4}$$

where ρ_t, the film resistance per unit area is called tunnel resistivity [11]. The tunnelling effect is temperature independent [11] and very sensitive to the film thickness [10]. As a voltage is applied to the film, electrical breakdown occurs with a field strength typically of the order of 10^8 V m^{-1} [11]. The film may also possibly be disrupted mechanically by contact force, which is called mechanical breakdown [11].

From equation (1), the dynamic resistance during RSW is the result of the sum of bulk resistance, constriction and film resistances, and the dominance of each component may change during the welding sequence. For example, the passage of welding current would reduce the resistance by breaking down the film but might increase the resistance by increasing temperature and hence the resistivity.

First in 1938, Hess and Ringer [8] showed that during RSW of polished stainless steel the sheet-to-sheet dynamic resistances rose initially to a maximum and subsequently fell to a lower value due to the formation and growth of a molten weld nugget. Since an ac power supply was used in this study and the resistances were calculated from measurement of peak current and peak voltage at each half cycle on oscillograms, the resolution of the dynamic resistance curve was low. In 1951, Roberts [12] observed the breakdown of contact resistance caused by the passage of a single cycle of high magnitude current on stainless steel and low carbon steel specimens. His study also showed that during the formation of a nugget in stainless steel, a continuous decrease in dynamic resistance was observed. The dynamic resistance curve for low carbon steel welds showed that after the breakdown of contact resistance, the resistance rose to a maximum and subsequently fell to a lower value, which becomes the basis for quality control strategies [4].

Later, in 1980, Dickinson *et al* [2] proposed six stages to characterize the dynamic resistance during welding of steels based on the competition between bulk resistance and contact resistance (figure 2). In stage I, the initial generation of heat would be concentrated at the surfaces due to the existence of surface contaminants. This heating caused the surface contaminants to break down, resulting in a very sharp drop in resistance. In stage II, the asperity softening caused the resistance to continue to decrease, but the increasing temperature resulted in an increase in the resistivity, thus providing the opposite effect. In stage III, the increase in bulk resistivity resulting from increasing temperature dominated the resistance curve. In stage IV, melting occurred, the dynamic resistance curve reached a β peak at which resistance started to drop due to molten nugget growth, and mechanical collapse overcame the resistance rise resulting from increasing temperature. In stage V, the growth of the molten nugget and mechanical collapse continued to cause the resistance to decrease. If the nugget grew to a size such that it could no longer be contained by the surrounding solid metal under the compressive electrode force, expulsion would occur resulting in a sudden drop in dynamic resistance.

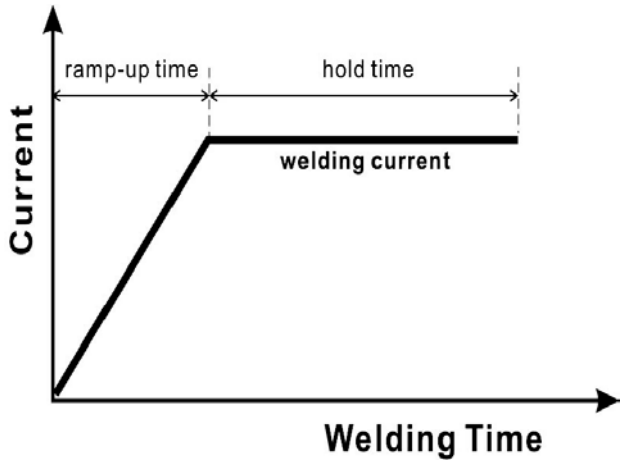

Figure 3. Current waveform.

3. Experimental procedure

Nickel sheets (Ni 200, annealed) 0.2 mm in thickness were used in this study. Lap-welded joints were made using coupons approximately 40 mm long and 8 mm wide. The two sheets were placed such that their rolling directions were parallel to each other. Prior to welding, the samples were cleaned for 10 min in acetone using an ultrasonic cleaner.

A dc welding power supply MacGregor DC4000P was applied in this study. The weld head was Unitek 80A/115 (air activated). Flat-ended round RWMA Class 2 (Cu–Cr) electrodes 3.2 mm in diameter were used. The experimental set-up is shown in figure 1. The initial static resistance was measured using a digital micro-ohmmeter after welding force was applied but before the welding current was initiated. Dynamic signals were monitored by a data acquisition system controlled by a PC running MATLAB. A standard resistor R_s was in series in the welding current loop, the voltage drop through the resistor U_s was recorded by the data acquisition system. The welding current was computed as $I = U_s/R_s$. The voltage drops through the electrode-to-sheet and sheet-to-sheet interfaces were recorded as U_1, U_3 and U_2. The dynamic resistances through the three interfaces were calculated as $R_1 = U_1/I$, $R_2 = U_2/I$ and $R_3 = U_3/I$, respectively. Welding current was applied as shown in figure 3 with a ramp-up time of 22 ms and hold time of 99 ms. The welding force was 51 N. As-welded joints were peeled and the bond area diameters were estimated from the fractured faying surfaces and/or pulled-out buttons using the scanning electron microscope (SEM).

4. Results

Figure 4 shows the sheet-to-sheet dynamic resistances at welding currents of 1600 A (sample 1) and 2200 A (sample 2), in which the identical ramp-up time at 22 ms resulted in a rate of current increase before reaching the welding current at 73 A ms^{-1} and 100 A ms^{-1} for samples 1 and 2, respectively. Both dynamic resistance curves showed a peak in the initial stage with initial static resistances at 0.27 mΩ and 0.29 mΩ, respectively, for samples 1 and 2. A second peak was seen in the curve for sample 2 but not for sample 1. The examination of

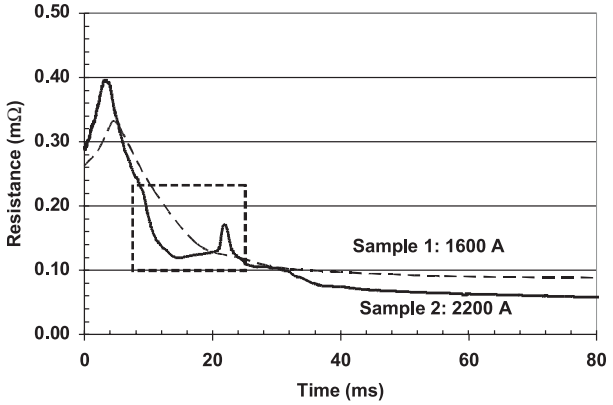

Figure 4. Sheet-to-sheet dynamic resistances with different welding current levels.

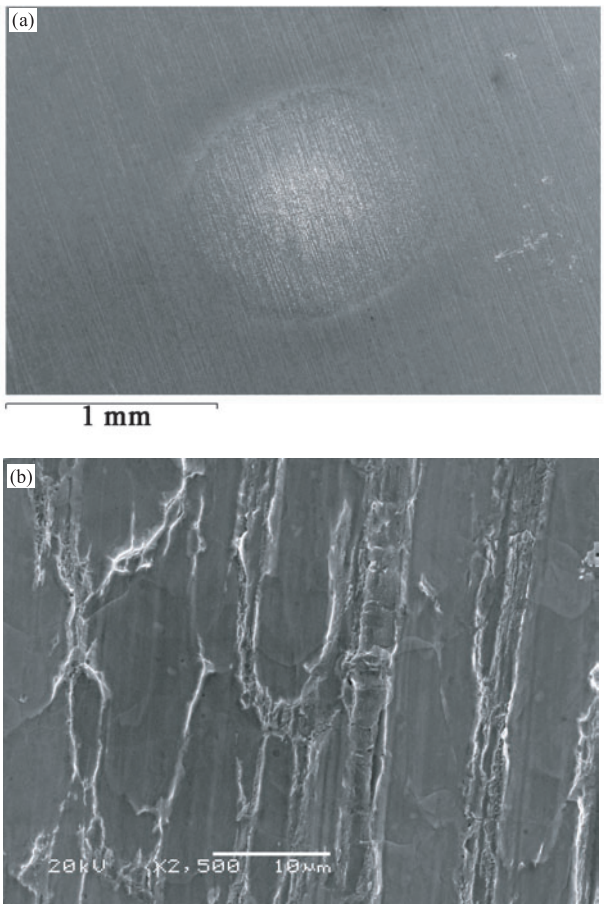

Figure 5. Low magnification photo (*a*) and high magnification photo (*b*) of fractured faying surface of sample 1 in figure 4, made with 1600 A welding current.

fractured faying surfaces after welding showed that only partial surface melting [13] occurred with sample 1 (figure 5, indicated by fractured local welds at asperity peaks). For sample 2, a 1.00 mm diameter nugget was formed and expulsion was observed at the faying surface (figure 6). This may indicate that the second peak was associated with the formation of the fusion nugget.

The next step was to investigate the first resistance peaks in figure 4. It was first observed that, as the welding current

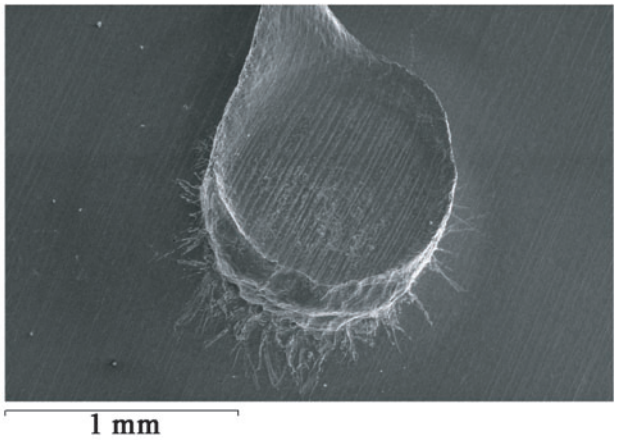

Figure 6. Pulled-out button of sample 2 in figure 4, made with 2200 A welding current.

ramped up from time zero, the sheet-to-sheet voltage drops were very close for samples 1 and 2 at the first resistance peaks (0.160 V and 0.171 V, respectively). Additional measurements at different welding currents were then made of the voltage drops at the first resistance peaks. The results were very interesting: voltage drops were very consistent at 0.163 ± 0.013 V (the mean plus and minus one standard deviation, based on 16 samples, including samples 1 and 2 in figure 4). These voltage drops were believed to be electrical breakdown voltages, which, according to O'Dwyer's work [14], should be a property of the film thickness. Nine additional samples were thus annealed at 573 K for 40 min in air to grow the surface oxides to investigate the effect of annealing on the voltage drops. The results were again very close, being 0.231 ± 0.018 V. This test provided further confirmation that these voltage drops may be electrical breakdown voltages.

A group of joints (of as-received sheets) was then made with the same welding current of sample 2 (at 2200 A) but the welding process sequences were terminated at different instants to further investigate the relationship between the nugget formation and dynamic resistance. The initial static resistances were, based on 11 samples, about 0.211 ± 0.053 mΩ. The dynamic resistance results are shown in figures 7–13 and described below. For better clarity, the dynamic resistance curves were expanded in the dashed rectangle range marked in figure 4.

According to figure 4, the dynamic resistance of sample 2 increased as the current was applied and reached the first peak at about 4 ms welding time (counting from time zero), then started to drop. When the welding current was shut down at 9 ms, the dynamic resistance curve experienced the first peak and reached the dropping stage (figure 7(*a*)). There was little visible change at the contact area compared with the unwelded surface (figures 7(*b*) and (*c*)). The decrease in dynamic resistance at this stage is believed to be due to the film breakdown at the contact surfaces.

When the welding current was shut down at 11 ms, the dynamic resistance curve was still at the dropping stage (figure 8(*a*)). SEM examination indicated that the asperities at the contact surface were flattened (figure 8(*b*)), but little evidence of melting was found in the contact area. The decrease in dynamic resistance at this stage is believed due to the softening of the asperities under elevated temperature, so that the actual contact area increased hence lowering the contact resistance.

When the welding current was shut down at 14 ms, the dynamic resistance curve was still at the decreasing stage, but it ran into a slowly dropping range (figure 9(*a*)). Partial surface melting was found to have occurred at the faying surface (figure 9(*b*)). When the welding current was shut down at 18 ms, the dynamic resistance curve showed the tendency of rising (figure 10(*a*)). A fusion nugget of 0.35 mm diameter was formed at the faying surface (figure 10(*b*)). This suggests that the valley point of the dynamic resistance curve is where the fusion nugget started to form. When the welding current was shut down at 19 ms, the dynamic resistance curve reached the rising stage after the valley point (figure 11(*a*)). The fusion nugget diameter increased to 0.58 mm (figure 11(*b*)). When the weld current was shut down at 20 ms, the dynamic resistance curve appeared to reach its second peak (figure 12(*a*)). The fusion nugget diameter increased to 0.91 mm (figure 12(*b*)), which is about the maximum nugget size without expulsion that can be produced for this Ni sheet under this electrode tip size and electrode force set-up. According to figures 10–12, the increase in dynamic resistance in this stage was mainly due to the growth of the fusion nugget.

When the weld current was shut down at 21 ms, the dynamic resistance curve started to drop after the second peak (figure 13(*a*)). The fusion nugget diameter was 0.97 mm, and metal expulsion was observed at the faying surface (figure 13(*b*)). It can be concluded that this drop was due to the expulsion, similar to what is observed in LSRSW [2], which caused the loss of molten metal, so that the thickness of the sheet at the weld position decreased, resulting in shortening of the current path.

5. Discussion

5.1. Static resistance

As mentioned above, the measured resistance between the two sheets includes one sheet-to-sheet contact resistance and the effective bulk resistance of one sheet. According to a numerical calculation on 0.2 mm thick mild steel sheets [15], the initial sheet-to-sheet apparent contact radius for mild steel is about 2.4 mm. Since the elastic modulus of Ni is equal to that of mild steel (table 1), it is believed that the initial sheet-to-sheet apparent contact radius for Ni sheets was about 2.4 mm in this experiment. With the sheet thickness at 0.2 mm and the resistivity of Ni at room temperature at 0.692×10^{-7} Ω m (table 1), the bulk resistance is about 0.0008 mΩ calculated from equation (2). It is obvious that the majority of the initial resistance (about 0.15–0.26 mΩ, see the previous section) was contact resistance. This is consistent with the observation in LSRSW of steels [12] that contact resistance dominates initial static resistance and plays a very important role in the initial stage of the welding process.

In the milder environments, the film on Ni is largely, if not exclusively, NiO of perhaps a limiting thickness of 30–50 Å. It has been assumed that this remains as a passivating film which grows no further [16]. The NiO film is as

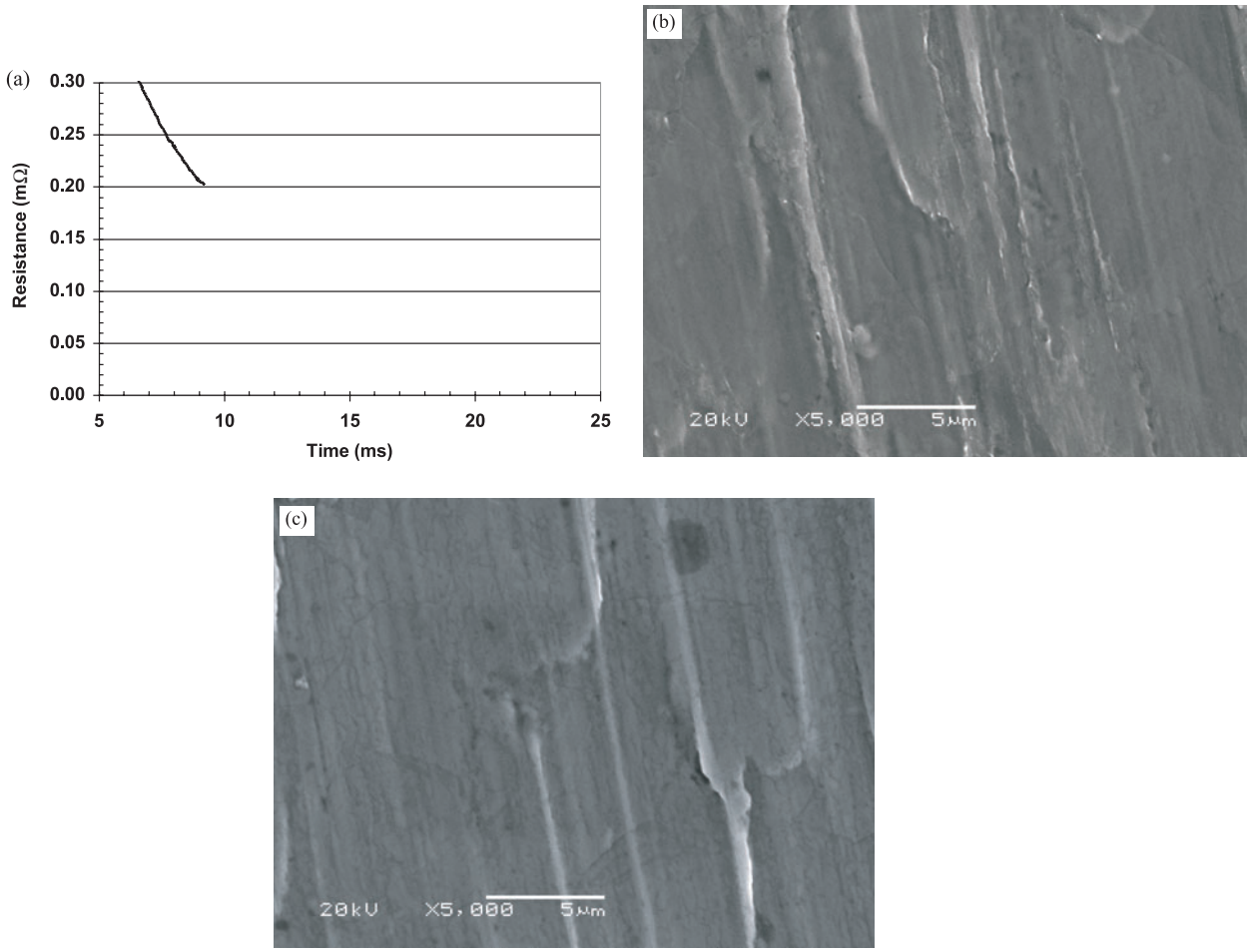

Figure 7. Sheet-to-sheet dynamic resistance curve (*a*) and the faying surface of sample made with 9 ms welding time (*b*) as well as unwelded surface (*c*).

strong as the metal. It scarcely ruptures at contact make [10]. Holm has measured the contact resistance of crossed rod nickel cylinders of 2 mm diameter at room temperature, and the tunnel resistivity of nickel oxide film was calculated based on elastic contact and plastic contact. For elastic contact, the tunnel resistivity of nickel oxide film ρ_t is about $54 \times 10^{-13}\,\Omega\,m^2$. While for plastic contact, ρ_t is about $92 \times 10^{-13}\,\Omega\,m^2$ [10]. It has been shown that asperity deformation is generally plastic in most practical applications [16]. Therefore, the plastic tunnel resistivity value is taken for consideration in equation (4), and the calculated film resistance for nickel at room temperature in this experimental set-up will be about 0.09 mΩ. According to equation (3), provided $\xi = 0.7$, $n = 10$–20, $F = 51$ N, $H = 6.9 \times 10^8\,N\,m^{-2}$ (table 1), the constriction resistance of nickel at room temperature will be 0.04–0.06 mΩ. Therefore, the sheet-to-sheet initial resistance was estimated using equation (1) to be 0.13–0.15 mΩ, which is close to the measured values.

To further investigate the initial behaviour of film and constriction resistance components, an assembly with the static resistance of 0.23 mΩ was subjected to only the first 5 ms of the 2200 A welding current programme. The dynamic resistance curve experienced the first peak and reached the dropping stage (curve I in figure 14). The welding force was left applied to this joint assembly, and without moving the specimen, after 1 min for heat to conduct away, the static resistance was then measured to be 0.11 mΩ. A second 5 ms welding current impulse was then re-applied on the same assembly, and the dynamic resistance appeared as curve II in figure 14. The static resistance was found to maintain at 0.11 mΩ after repeating the same current impulse for 5 times at a frequency of once per minute. This suggested that the 5 ms current impulse only broke the oxide film without causing asperity softening. SEM examination showed that there was little visible change at the contact area compared with the unwelded surface, this confirms the above idea and suggests that the film resistance for this assembly was about $0.23 - 0.11 = 0.12$ mΩ. The film resistance for pairs of this sheet material, based on 15 samples, was measured to be about 0.134 ± 0.027 mΩ. Clearly, the peak in dynamic resistance curve I in figure 14 was due to the film breakdown at the contact surfaces. The comparisons between the measurements and the calculations are summarized in table 2.

5.2. Dynamic resistance

The dynamic resistance during RSW, based on equation (1), is really the result of the changes in bulk and contact resistances. As welding progresses, the breakdown of surface films will cause a decrease of dynamic resistance. The resistivity of

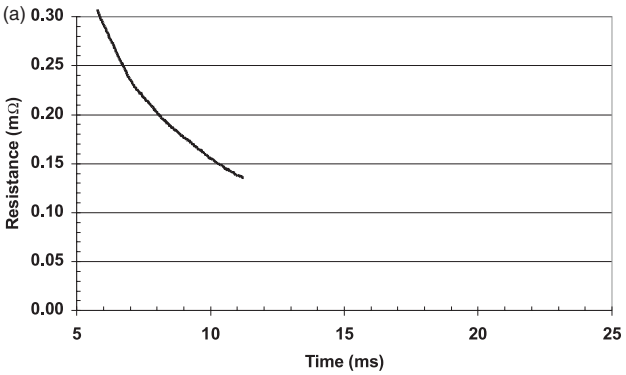

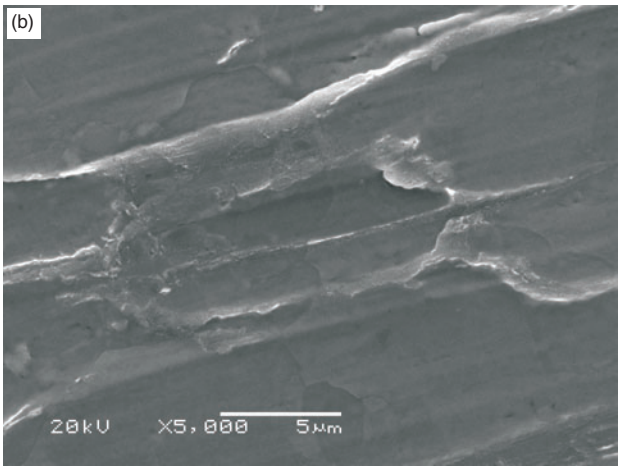

Figure 8. Sheet-to-sheet dynamic resistance curve (*a*) and the faying surface (*b*) of sample made with 11 ms welding time.

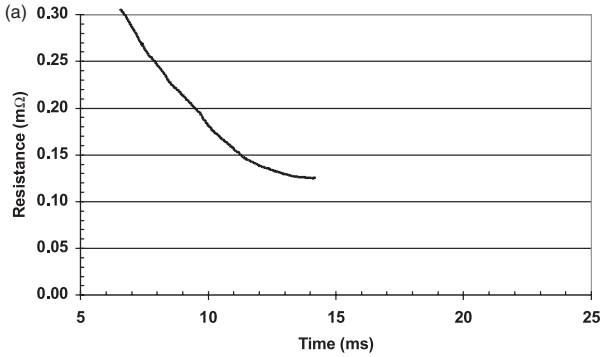

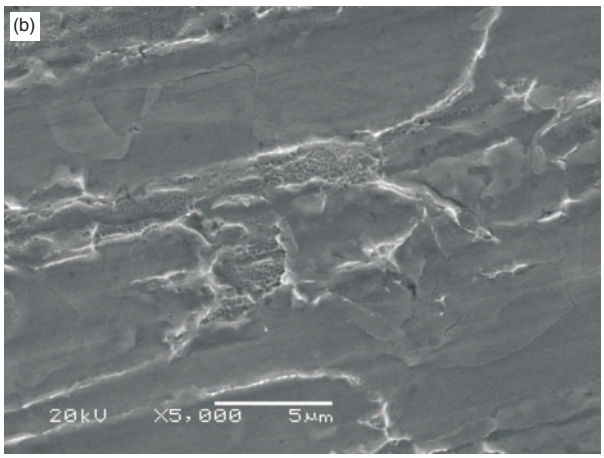

Figure 9. Sheet-to-sheet dynamic resistance curve (*a*) and the faying surface (*b*) of sample made with 14 ms welding time.

bulk material and asperities will increase because of increase of temperature, resulting in increase of dynamic resistance. The softening of asperities occurs causing increase of contact area thus decreasing the dynamic resistance. The solid to liquid phase transformation of Ni during nugget formation will subsequently increase dynamic resistance because there is a large resistivity difference between solid Ni and liquid Ni at the melting temperature (figure 15). These changes provide a physical basis to divide the dynamic resistance R into the following stages (figure 16): (1) asperity heating; (2a) surface breakdown; (2b) asperity softening; (2c) partial surface melting; (3) nugget growth and (4) expulsion. For clarity, a different numbering system was introduced in the dynamic resistance curve of SSRSW. Instants A, B and C and stages 1, 2, 3 and 4 were used in SSRSW instead of instants α and β and stages I, II, III, IV and V, as used in LSRSW (figure 2) [2]. The relative contributions to dynamic resistance of dynamic film resistance R_F, constriction resistance R_C and bulk resistance R_B during a welding sequence are illustrated schematically in figure 16, which also shows the process stages and time instants defined above.

5.2.1. Stage 1. When the welding current passed, the contact spots were first heated although the bulk material would still be cool. According to equation (3), the constriction resistance would increase as temperature increases, since the resistivity increases with temperature. This would cause an

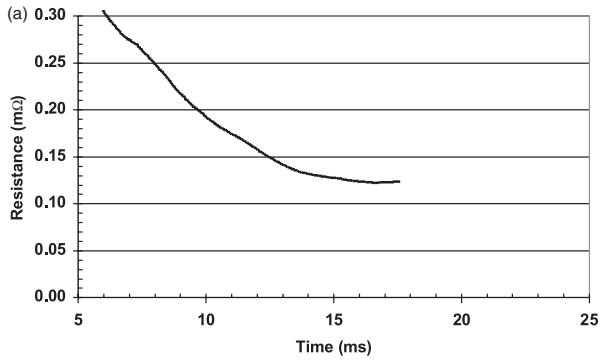

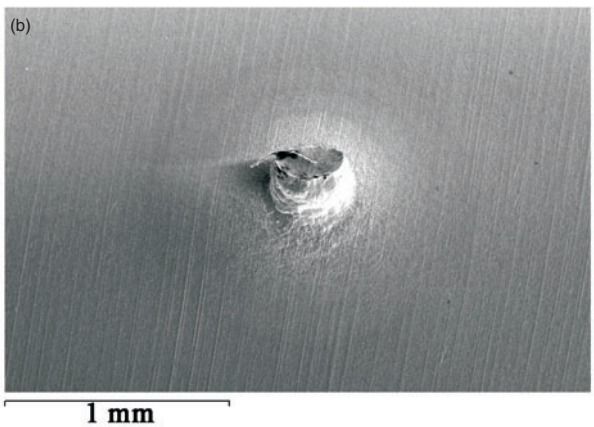

Figure 10. Sheet-to-sheet dynamic resistance curve (*a*) and the pulled-out button (*b*) of sample made with 18 ms welding time.

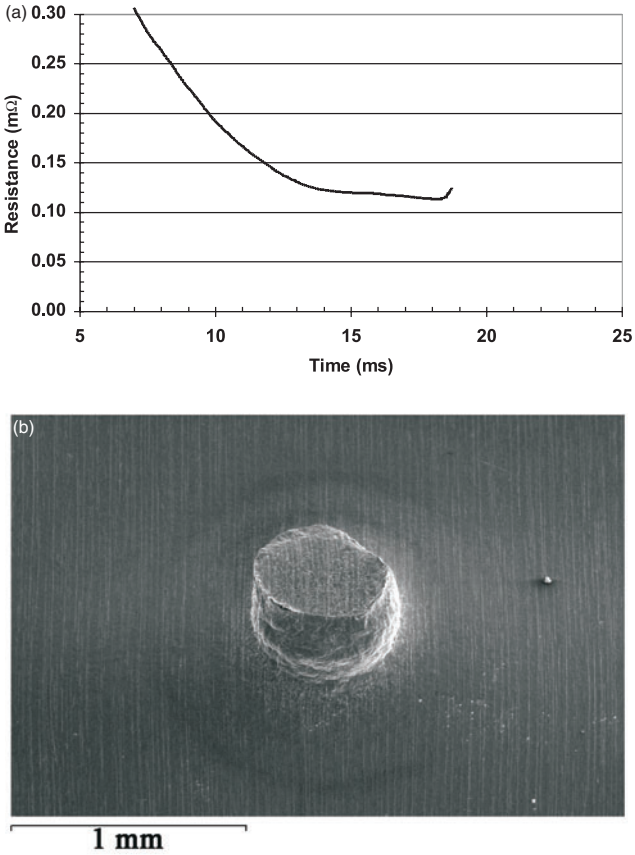

Figure 11. Sheet-to-sheet dynamic resistance curve (*a*) and the pulled-out button (*b*) of sample made with 19 ms welding time.

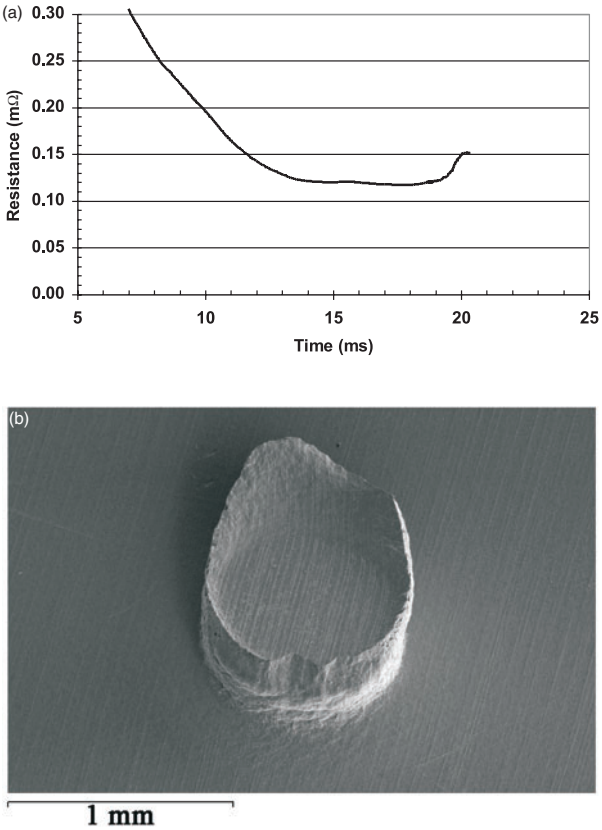

Figure 12. Sheet-to-sheet dynamic resistance curve (*a*) and the pulled-out button (*b*) of sample made with 20 ms welding time.

increase in dynamic resistance because the initial resistance was dominated by contact resistance.

Due to its face-centred cubic crystal structure, the hardness of nickel shows little change with temperature lower than its softening temperature [17], and no obvious microstructural change was observed on the faying surfaces after welding until long after the first resistance peaks (figure 7), it is reasonable to assume that the temperature built up at the first stage was much lower than the softening temperature (table 1) and that the contact status did not change. Assuming the temperature built up was 773 K at the contact spots and the bulk material remained was much lower than 773 K, the only visible changed component of R in this stage is R_C. Application of the material properties (table 3 and figure 15) to equation (3) produced a predicted sheet-to-sheet resistance increase of 0.19–0.26 mΩ. This is much higher than the resistance increase observed at the initial stage (e.g. about 0.08–0.10 mΩ in figure 4). This confirms that the temperature increases at the faying surfaces were lower than the softening temperature (table 1).

However, this heating stage has usually been missed in the observations during previous LSRSW process studies (figure 2). The main reason may be that, in general, surface conditions are less clean in LSRSW than in SSRSW. When Ni sheets after annealing at 573 K in air for 40 min were used to make joints at the same current of sample 2 (2200 A, 22 ms ramp-up time), the dynamic resistance curve appeared as sample 3 in figure 17. Comparing the curve for sample 3

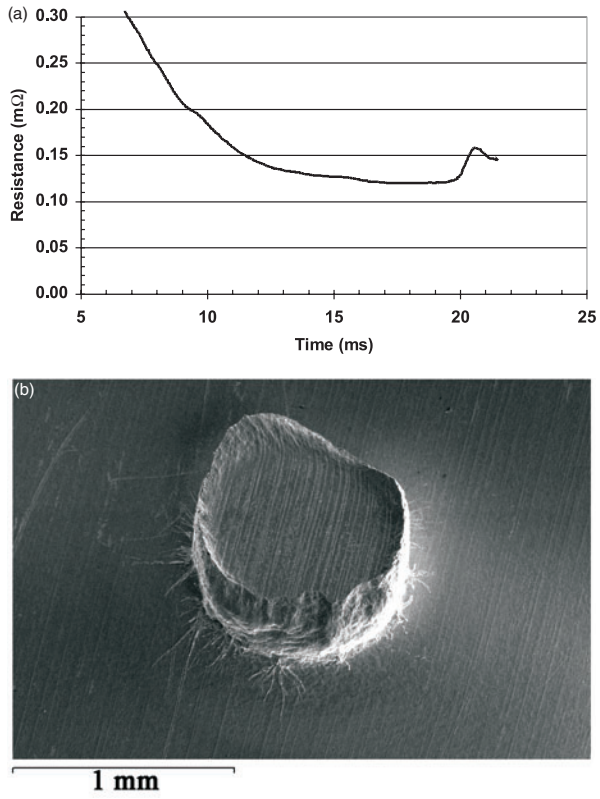

Figure 13. Sheet-to-sheet dynamic resistance curve (*a*) and the pulled-out button (*b*) of sample made with 21 ms welding time.

Table 1. Material properties [11, 21].

	Softening temperature (K)	Melting temperature (K)	Room temperature resistivity (Ω m)	Hardness ($N\,m^{-2}$)	Elastic modulus ($N\,m^{-2}$)
Ni	793	1728	0.684×10^{-7}	6.9×10^{8}	1960×10^{8}
Fe	773	1808	0.97×10^{-7}	5.9×10^{8}	1960×10^{8}

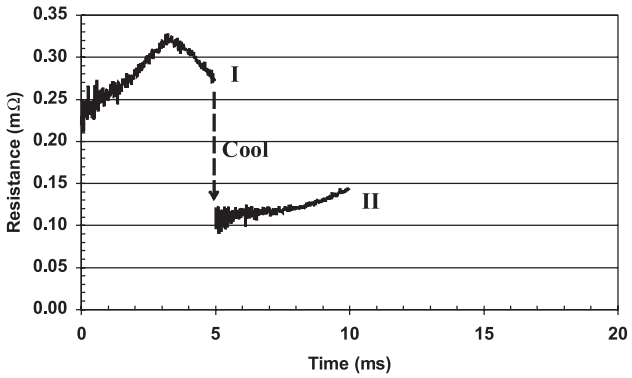

Figure 14. Sheet-to-sheet dynamic resistance curve of sample made with 5 ms welding time of the 2200 A programme.

Table 2. Static resistances.

	Theory (mΩ)	Experimental (mΩ)
R_F	0.09	0.11–0.16
R_C	0.04–0.06	—
$R_F + R_C$	0.13–0.15	0.15–0.26

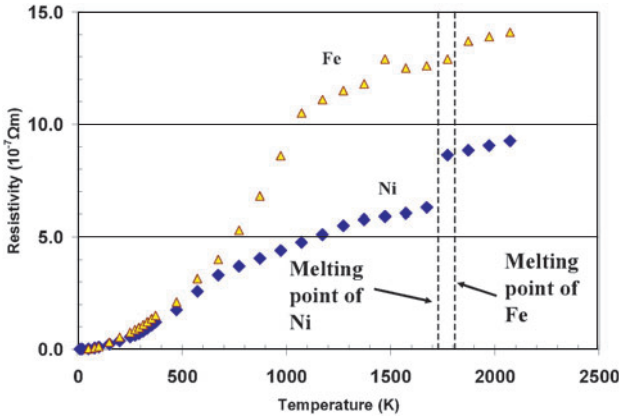

Figure 15. Resistivity plotted against temperature for pure Ni and Fe [21].

(This figure is in colour only in the electronic version)

in figure 17 and for sample 2 in figure 4, the first heating stage was missed for sample 3. This suggests that at the same current setting, the thicker the surface oxide, the more difficulty would be experienced in observing the first resistance peaks. A careful literature study indicated just one LSRSW case in which the first resistance peaks were visible. This was a study on LSRSW of degreased and pickled steels [18], in which a small peak appeared at the initial stage followed by a β peak in the dynamic resistance curve; the initial peak did not appear on as-received steels. However, the author did not clearly identify

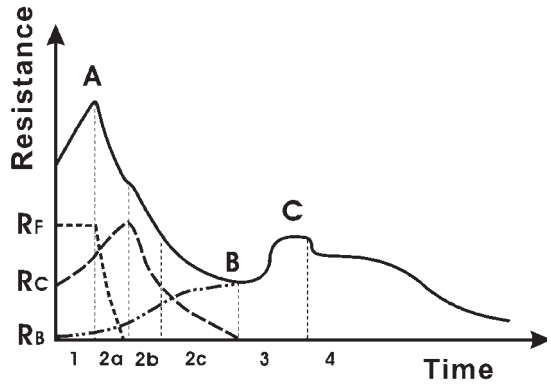

Figure 16. Schematic showing a typical sheet-to-sheet dynamic resistance curve during SSRSW of Ni (solid line) and its components (broken line).

this peak or perform further study. It therefore appears that the initial dynamic resistance peak will only be visible when surface films are present but they are thin enough and the current increase rate is low enough so that significant asperity heating occurs before the occurrence of film breakdown.

A related reason for the missing of the initial stage before film breakdown in LSRSW is that the welding currents in LSRSW are mostly ac, with which the rate of current increase is very fast. As shown in figure 17, with the same annealed material, the first peak was only observed at a slow rate of current increase for sample 4 ($2\,A\,ms^{-1}$) but not at the fast rate of current increase for sample 3 ($100\,A\,ms^{-1}$). As mentioned above, the breakdown voltage for an annealed sample is about 0.231 V. According to the dynamic resistance curve for sample 4 (figure 17), the film started to break down when the dynamic resistance reached about 5.5 mΩ. Meanwhile, when the current reached about 42 A ($I = U/R$, I is the current, U is the voltage drop, R is the resistance), the film started to break down. For a current rising from zero at a rate of $100\,A\,ms^{-1}$, the breakdown instant will be at 0.42 ms, so that the heating stage would be missed for sample 3 due to the limited resolution of the measurement instrument. For a current rising from zero at a rate of $2\,A\,ms^{-1}$, the breakdown instant will be at about 21 ms, allowing the asperity heating stage to be captured by the instrument. Most dynamic resistance measurements in LSRSW have used ac currents, in which the rate of current increase was at the order of $2000\,A\,ms^{-1}$. It was observed in this work that, even in SSRSW using ac with a rate of current increase in the order of $500\,A\,ms^{-1}$, no first peak was observed on as-received Ni sheets.

5.2.2. Stage 2a. In this stage, the dynamic resistance dropped because of electrical breakdown of surface films (figure 16). Under normal conditions, surface films (oxide layers or other contaminants) will exist on the sheet surface. As mentioned

Table 3. Resistivity of nickel at different temperatures [21].

Temperature	Room temperature (Ω m)	573 K (Ω m)	773 K (Ω m)	1673 K (Ω m)	1773 K (Ω m)
Resistivity	0.684×10^{-7}	2.58×10^{-7}	3.7×10^{-7}	6.3×10^{-7}	8.63×10^{-7}

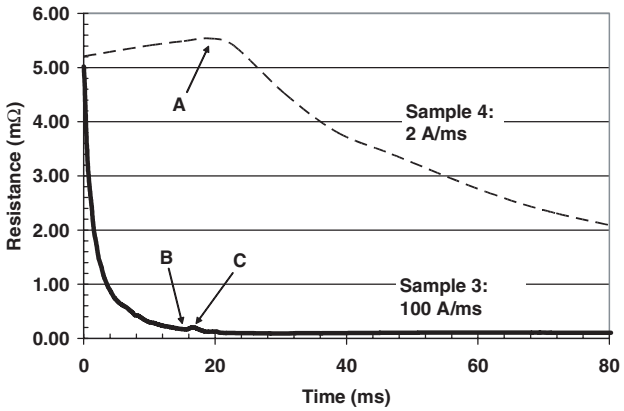

Figure 17. Sheet-to-sheet dynamic resistance curves for Ni samples annealed at 573 K for 40 min in air.

earlier, in the milder environments, the film on nickel is largely, if not exclusively, NiO of perhaps a limiting thickness of 30–50 Å [16]. Electrical film breakdown for NiO occurs with a field strength of (1.1–1.4) $\times$ 10^8 V m^{-1} [10]. Therefore in theory, applying a potential of 0.3–0.7 V on the contact interface will cause film breakdown at the nickel-to-nickel interface. In figure 4, the dynamic resistances for both samples were found starting to decrease when the sheet-to-sheet voltage drop reached about 0.16 V, which is slightly lower than the predicted breakdown voltage based on a flat dielectric film. This may be due to field enhancement by small projecting asperities [11], so that the required breakdown voltage is lower than the predicted value. When the breakdown occurs, the film resistance will decrease (figure 16). This will result in a very sharp drop in dynamic resistance and is very similar to the stage I in LSRSW (figure 2) [2], in which the film would break down mechanically or electrically.

5.2.3. Stage 2b. This stage is similar to stage II of figure 2 [2], in which, as heating progressed, the asperities softened and the real contact area increased thus causing contact resistance and hence dynamic resistance to continue to drop. However, in LSRSW (figure 2), the competition between contact and bulk resistances results in an increase in dynamic resistance later after instant α since the contact resistance disappears very quickly under the resistance heating and large compressive force. At the same time, the resistivity of the sheet material increased with increasing temperature and hence caused an opposite effect. As temperature increased, the contribution of bulk resistance to dynamic resistance would gradually be higher than that of contact resistance and finally determined the tendency of dynamic resistance. On the other hand, in SSRSW, since the dynamic resistance was still dominated by contact resistances (because of the relatively low surface compressive pressure [15]), the overall behaviour of dynamic resistance reflected the tendency of growth of contact area and decreased continually at this stage.

5.2.4. Stage 2c. In this stage, the dynamic resistance, apparently affected increasingly by bulk resistance, continued to drop but at a much lower rate and eventually reached its minimum. This is different from LSRSW, in which bulk resistance dominates the dynamic resistance soon after softening occurs and thus dynamic resistance increases, reflecting the tendency of increasing bulk resistance (figure 2, stages II and III). In SSRSW, the contact resistance may not dominate the dynamic resistance after melting begins, but it remains significant up to this point, again due to the related low electrode force and faying surface compressive stress used in SSRSW compared with that in LSRSW. As the heat built up, some contact spots started to melt and the contact area continued to increase, so that the contact resistance decreased. However, in its liquid phase Ni has much higher resistivity than solid Ni (figure 15), also the sheet bulk resistance increases at higher temperature, offsetting the effect of area increase: the rate of decrease of dynamic resistance reduced and finally reached the valley point B (figure 16).

5.2.5. Stage 3. After the B valley (figure 16), most contact resistance should have disappeared and the dynamic resistance began to reflect essentially the behaviour of bulk resistance. Since there is large resistivity difference between liquid and solid Ni phases (figure 15), as the fusion nugget formed and grew, the dynamic resistance increased correspondingly until the nugget reached its maximum diameter and/or thickness at the C instant.

At the B valley, since the surface started to melt, the bulk temperature was very close to the melting point. According to a numerical calculation [15], the sheet-to-sheet contact diameter at this stage would be about 1.3 mm. Assuming the central portion of the joint as a solid cylinder at 1.3 mm in diameter and 0.2 mm in length, the sheet-to-sheet bulk resistance would be about 0.095 mΩ by equation (2) using resistivity value at 6.3×10^{-7} Ω m (table 3 and figure 15). As a comparison, the experimental observations in this work (e.g. figures 4, 10(*a*), 11(*a*), 12(*a*) and 13(*a*)) indicated that those minimum resistances were about 0.10–0.13 mΩ, only slightly higher than the predicted 0.095 mΩ, because there was a thin layer of higher resistivity liquid Ni between two sheets.

At the C peak, the nugget was almost at its maximum at diameter of 1.0 mm. Assuming the central portion of the joint as a liquid cylinder at 1.0 mm in diameter and 0.2 mm in length, the sheet-to-sheet bulk resistance would be about 0.22 mΩ by equation (2) using resistivity value at 8.63×10^{-7} Ω m (table 3 and figure 15). This is slightly higher than the experimental observations (e.g. figures 4, 12(*a*) and 13(*a*), 0.15–0.18 mΩ), which is due to the surrounding contacted solid providing a shunting path for the current. In LSRSW of mild steel, the effect of macro mechanical collapse is normally so effective that the dynamic resistance starts to drop at the instant β before the nugget reaches maximum size, because the electrode pressure in LSRSW is much higher than that in SSRSW.

The difference between the B and C in this work (figures 4, 12 and 13) is about 0.04 mΩ, which is very close to the difference between α and β in LSRSW of mild steel, at about 0.03 mΩ [12]. Similar to the case in LSRSW, the dynamic resistance curve of SSRSW of Ni could also be used in quality control since the features of nugget formation are similarly obvious.

5.2.6. Stage 4. When energy input is too high, the surrounding solid material cannot hold the liquid phase and weld metal expulsion occurs [2]. The bulk resistance shows a sudden drop (figure 16) due to loss of material causing the shortening of the current path. Then the rate of heat generation ($q = I^2R$) decreases, the temperature starts to drop, although the welding current continues to pass. The decrease in temperature in turn lowers the bulk resistivity and promotes the decrease of dynamic resistance until the heat generation and heat dissipation reach an equilibrium state. Another factor contributing to the reduction of dynamic resistance in the final expulsion stage is, as the surrounding material continues to collapse, the sheet-to-sheet contact area increases, so that the dynamic resistance is further decreased. While there is no direct experimental proof of the above sequence, the research on FEM simulation of SSRSW of mild steel [15] showed that the temperature started to drop after the 4th cycle, which is consistent with the dynamic resistance curve in this work.

Bhattacharya and Andrew [19] has predicted that the dynamic resistance curve during RSW of nickel will be very similar to that during LSRSW of mild steel due to their close softening temperature, melting temperature and resistivity (table 1). However, there is an extra initial peak in the dynamic resistance curve for SSRSW of Ni mainly due to the clean Ni surface and the relatively low rate of current increase. In addition, the times of melting onset are different between SSRSW of Ni and LSRSW of steels possibly due to the much lower electrode force used in SSRSW. Also, the difference in electrode force and resistivity curve (figure 15) may result in the maximum nugget size being reached at instant C during SSRSW of Ni (figure 16), while the maximum nugget is formed after instant β during LSRSW of mild steel (figure 2).

Gedeon and Eagar [20] had shown that the electrode-to-electrode dynamic resistance curve during LSRSW of Zn-coated steel reflects the resistance change of the electrode-to-sheet interface as well as the resistance change of the sheet-to-sheet interface. This makes it difficult to use the electrode-to-electrode dynamic resistance as a quality control input variable. In this work on SSRSW of Ni, the shape of the electrode-to-electrode dynamic resistance curve was found to be very similar to the sheet-to-sheet dynamic resistance curve (figure 18). Most importantly, the electrode-to-electrode dynamic resistance curve during SSRSW of Ni indicates the state of nugget formation and could be used for quality control.

6. Conclusions

The dynamic resistance during SSRSW of Ni has been investigated. Variation of the welding current waveform and material surface condition, and correlation of electrical measurements with observed material surface changes, have permitted resolution of the rather complex physical phenomena that occur during the welding sequence. The following stages were defined based on the physical changes occurring in the workpieces during the welding process: asperity heating, surface breakdown, asperity softening, partial surface melting, nugget growth and expulsion. The major conclusions are summarized as follows:

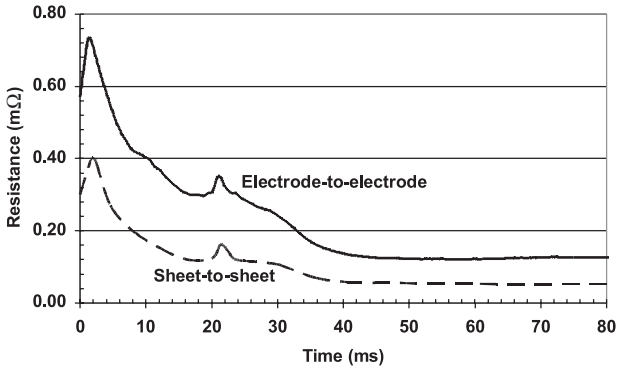

Figure 18. Sheet-to-sheet and electrode-to-electrode dynamic resistance curves of Ni.

1. At room temperature, the sheet-to-sheet static resistance as measured in a set-up for SSRSW of thin Ni sheet is dominated by sheet-to-sheet contact resistance.
2. An asperity heating stage causing an initial increase and peak in the dynamic resistance curve was observed during SSRSW of Ni under low rate of current increase. This effect, which has rarely been seen and not previously explained in RSW studies, is specifically associated with relatively clean surfaces with thin surface films and low current increase rate.
3. Surface film breakdown during SSRSW of Ni was found to occur at a definite voltage drop whose magnitude depended on the thickness of the surface oxide.
4. Surface asperities began to soften and constriction resistance to decrease shortly after the moment of film breakdown. However, lower electrode pressures in SSRSW were found to cause persistence of constriction resistance effects on the evolution of dynamic resistance until near the beginning of nugget initiation.
5. The times of melting onset and maximum nugget formation during SSRSW of Ni are different from those during LSRSW of mild steel because of the difference in electrode force and material resistivity.
6. A second peak was observed in the dynamic resistance curve during SSRSW of Ni indicating the formation of a fusion nugget, and this could be used as quality control input variable.

Acknowledgments

This work has been supported by the Natural Sciences and Engineering Research Council (NSERC), Canada.

References

[1] Resistance Welder Manufacturers Association 1989 *Resistance Welding Manual* 4th edn (Philadelphia: RWMA)

[2] Dickinson D W, Franklin J E and Stanya A 1980 *Weld. J.* **59** 170S
[3] Kaiser J G, Dunn G J and Eagar T W 1982 *Weld. J.* **61** 167S
[4] Towey M and Andrews D R 1968 *Weld. Met. Fab.* **36** 383
[5] Zhou Y, Gorman P, Tan W and Ely K J 2000 *J. Electr. Mater.* **29** 1090
[6] Zhou Y, Dong S J and Ely K J 2001 *J. Electr. Mater.* **30** 1012
[7] Brown B M 1987 *Weld. J.* **66** 18
[8] Hess W F and Ringer R L 1938 *Weld. J.* **17** 39S
[9] Andrews D R and Bhattacharya S 1973 *Met. Constr.—Br. Weld.* **5** 172
[10] Holm R and Holm E 1967 *Electric Contacts: Theory and Application* 4th edn (New York: Springer)
[11] Baker D *et al* 1971 *Physical Design of Electronic System* vol 3 (Englewood Cliffs, NJ: Prentice-Hall)
[12] Roberts W L 1951 *Weld. J.* **30** 1004
[13] Tan W, Zhou Y and Kerr H W 2002 *Metall. Mater. Trans.* A **33** 2667
[14] O'Dwyer J J 1964 *The Theory of Dielectric Breakdown of Solids* (London: Oxford University Press)
[15] Chang B H and Zhou Y 2003 *J. Mater. Process. Technol.* **139** 635
[16] Slade P G 1999 *Electrical Contacts* (New York: Marcel Dekker)
[17] Dieter G E 1986 *Mechanical Metallurgy* (New York: McGraw-Hill)
[18] Savage W F, Nippes E F and Wassell F A 1978 *Weld. J.* **57** 43S
[19] Bhattacharya S and Andrew D R 1974 *Weld. Met. Fab.* **42** 296
[20] Gedeon S A and Eagar T W 1986 *Metall. Trans.* B **17** 887
[21] Tslaf A 1981 *Combined Properties of Conductors* (New York: Elsevier Scientific)